Geochemical Perspectives Letters

Fate of organic compounds during transformation of ferrihydrite in iron formations

S. Jelavić[1,2*], A.C. Mitchell[3], K.K. Sand[1,2,3]

OPEN ACCESS

doi: 10.7185/geochemlet.2030

Abstract

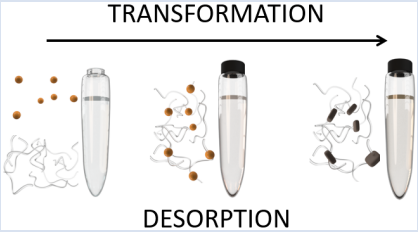

The absence of organic compounds from Precambrian iron formations (IF) challenges the hypothesis of the biogenic origin of IF. Here we address the fate of adsorbed organic compounds during transformation from ferrihydrite to hematite. We determined the binding energy between hematite and common molecular terminations found in extracellular polymeric substances and biofilms: carboxylic, hydroxyl and phosphate functional groups. We found that the bond between hematite and hydroxyl groups is approximately 2 times stronger than the bond between hematite-carboxyl and -phosphate groups. We transformed synthetic ferrihydrite to hematite at 90 °C in presence of glycerol, which has a high density of hydroxyl groups, and measured the amount of mineral associated glycerol before and after the transformation. We show that the transformation releases glycerol highlighting that organic compounds adsorbed at precursor ferrihydrite could be desorbed during the process of IF sedimentation and diagenesis. Our results suggest that the absence of organic compounds in IF should not be used as evidence against their biogenic origin.

Received 20 March 2020 | Accepted 7 August 2020 | Published 15 September 2020

Introduction

Traditionally, iron formations (IFs) have been considered as abiotically generated chemical sediments but an increasing body of evidence suggests the active role of microbes in their precipitation (Koehler *et al.*, 2010). The role of anoxygenic phototrophic bacteria in the formation of IFs has been the object of speculation since the work of Garrels *et al.* (1973). An improved understanding of microbially induced Fe(II) oxidation highlights that oxidising bacteria, such as *Rhodobacter ferrooxidans*, could likely drive the formation of IFs (Kappler *et al.*, 2005). Further, mass balance calculations have shown that Fe(II)-oxidising phototrophic bacteria have the capacity to oxidise all Fe(II) from the Precambrian ocean, causing formation of iron (oxyhydr)oxide (FeOx) (Hegler *et al.*, 2008). However, the low concentration of organic compounds in IFs and their diagenetic or metamorphic derivatives, challenges the hypothesis of their biogenic origin (Klein, 2005).

Extracellular polymeric substances (EPS) promote FeOx nucleation (Sand *et al.*, 2020) where microbially formed FeOx are often found in close association with the EPS (Chan *et al.*, 2004). When EPS is encrusted with FeOx, the polymers are shed and new EPS are formed. This prevents the encrustation of the microbe itself (Phoenix *et al.*, 2000; Chan *et al.*, 2004). During IF formation, FeOx-EPS composites would have settled through the water column and been deposited on the sea floor. Some of the organic compounds were degraded by diagenetic and metamorphic processes (Köhler *et al.*, 2013; Posth *et al.*, 2013; Halama *et al.*, 2016). In addition, there is evidence that the depositional environment was most likely scarce in organic compounds (Dodd *et al.*, 2019). Thus, the majority of the organic compounds was likely lost prior to deposition.

Hematite is a major component of IFs found today (Konhauser *et al.*, 2017) but, initially, the FeOx in the FeOx-polymer complexes were most likely composed of ferrihydrite (Chan *et al.*, 2004). The transformation to hematite would have happened in aqueous solutions both before (Sun *et al.*, 2015) and after deposition on the seabed. Depending on the solution conditions, ferrihydrite to hematite transformation can involve intermediary phases such as lepidocrocite and goethite, *e.g.*, through Fe(II) catalysed transformation (Hansel *et al.*, 2003), or it can be direct (Cudennec and Lecerf, 2006). Transformation involving intermediary phases is a dissolution-precipitation process (Schwertmann and Murad, 1983) implying that the interface between ferrihydrite and organic compounds is eliminated. In this scenario, organic compounds would have been released to solution where they could have been re-adsorbed but less strongly bound to newly formed phases (Chen *et al.*, 2015), or released in the water column and subsequently degraded by various biotic and abiotic processes (Kleber *et al.*, 2015). The direct transformation from ferrihydrite to hematite is a solid-state transition where atoms move only locally to occupy new structural positions (Cudennec and Lecerf, 2006), without the loss of an interface with adsorbed complexes. Thus, the direct transformation of ferrihydrite to hematite is not necessarily accompanied by a removal of organic compounds. However, the Gibbs free energy of binding (ΔG_{bu})

1 Nano-Science Center, Department of Chemistry, University of Copenhagen, Universitetsparken 5, Copenhagen, Denmark
2 Section for GeoGenetics, Globe Institute, University of Copenhagen, Øster Voldgade 5-7, Copenhagen, Denmark
3 Aberystwyth University, Department of Geography & Earth Sciences, Aberystwyth, UK
* Corresponding author (email: stanislav.jelavic@sund.ku.dk)

between ferrihydrite and EPS is larger than between hematite and EPS (Sand *et al.*, 2020) implying that the polymers were more likely to desorb from hematite than from ferrihydrite. In such a case, the absence of organic compounds in IFs cannot be an argument against their biogenic origin.

To understand better the fate of adsorbed organic compounds during direct transformation from ferrihydrite to hematite, we used dynamic force spectroscopy (DFS) to measure the energy of binding between hematite and representative organic functional groups found in EPS. Subsequently we identified the functional group least likely to desorb during transformation and carried out transformation experiments where we used thermogravimetric analysis (TGA) to measure the loss of organic compounds during transformation.

Materials and Methods

DFS. We used an Asylum MFP3D atomic force microscope (AFM) and functionalised gold coated AFM tips (MSCT, Bruker) with carboxyl (COO^-), hydroxyl (OH), and phosphate (HPO_4^-) headgroups pointing away from the AFM probe (Fig. 1a). Tips were functionalised following the protocol described in Jelavić *et al.* (2017) (details in SI).

We used the {0001} face for DFS because it is one of the most common hematite surfaces in the environment (Hartman, 1989) and because it is a predominant face on hematite produced by transformation of ferrihydrite (Cornell and Schwertmann, 2004). The specular hematite monocrystal {0001} face was cleaned prior to analysis following the protocol described in Jelavić *et al.* (2017) (details in the SI). For DFS measurements, we collected >500 force curves *per* experiment. The tip approaching velocity was set to 500 nms^{-1} and the retraction velocity varied between 10–10000 nms^{-1}. The trigger force was set to 100 pN and dwell time to 0.5 s. During the measurement, the head groups bound to the hematite surface (Fig. 1a) and we measured the forces applied to break the bond (*i.e.* the force curve, Fig. 1b). We fit the rupture forces *vs.* the loading rate to a multibond model (Friddle *et al.*, 2012) enabling calculation of ΔG_{bu} (Eq. S-1 to Eq. S-4). The measurements were done in 10 mM NaCl solution at pH = 5.6. We chose these conditions, rather than conditions at which the transformation experiments were conducted, to maximise the interaction forces between the tip and hematite surface (Lützenkirchen *et al.*, 2013; Newcomb *et al.*, 2017).

Transformation experiments. Ferrihydrite was synthesised using the method of Schwertmann and Cornell (2000). We used 0.5 M NaCl solution and pH = 7 as a proxy for Precambrian seawater. We chose glycerol (CH_2**OH**-CH**OH**-CH_2**OH**) as a model for an OH-rich molecule. Adsorption of polymers is a complex function of degree of branching, length and hydrophobicity (van Oss, 1997). The aim here is not to account for such variations but to isolate the effect of ΔG_{bu}, which is independent of those parameters, on the magnitude of desorption during transformation. Coprecipitation of ferrihydrite-polymer aggregates results in a high organic content compared to adsorbed polymers (Mikutta *et al.*, 2014) and can cause variations in grain size and aggregation. To avoid any influence from such variations and to avoid low transformation rates related to high surface coverage, we adsorbed glycerol to ferrihydrite in this study. We mixed 15 mg of ferrihydrite with 15 ml of 0.5 M NaCl and added glycerol to a final concentration of 0.5 % (Fig. 1c). In control samples, we omitted glycerol. Samples were shaken at 100 rpm overnight to equilibrate. The next day, a batch of samples was rinsed with 20 ml of rinsing stock solution (0.5 M NaCl adjusted to pH = 7 with 1 M NaOH) by ultra-centrifugation (equilibrated sample). Another batch was placed in the oven heated to 90 °C. The samples from the oven were sampled at specific time steps to follow the transformation pathway using X-ray diffraction (XRD). When sampled, a batch was rinsed with 20 ml of 0.5 M NaCl that was adjusted to pH = 7 (aged sample). All samples were freeze dried after rinsing.

XRD. Samples for XRD were washed with ultra-deionised water (resistivity >18.2 MΩcm). A volume of 1.5 ml of suspension was pipetted on the zero background Si holders and left to dry at room temperature. Such sample preparation results in large preferred orientation of anisotropic grains such as goethite and lepidocrocite and allows us to detect minute quantities of crystalline material in a poorly ordered matrix of ferrihydrite. We collected diffractograms in reflection mode on the Bruker D8 Advance instrument using Cu Kα radiation (λ = 1.5418 Å) operated at 40 kV and 40 mA, and a LynxEye detector. Diffractograms were collected from 10–90° 2θ with step size of 0.02° and 1.7 s counting time *per* step. The sample was spun at 20 rpm. We used 0.3° divergence and 3° antiscatter slits, 2.5° Soller slits on incident and diffracted beams and a 0.02 mm thick Ni-filter. The opening of detector window was 2.94°.

TGA. We used Netzsch TG 209 F1 Libra. Samples were heated at a rate of 10 °C min^{-1} from 30 to 1000 °C under N_2 atmosphere. ~15 mg of sample were placed into the Pt crucible and the weight loss was measured as a function of temperature.

TEM. Images were taken with a Philips CM 20 TEM equipped with a thermionic LaB_6 filament. We used an accelerating voltage of 200 kV. Samples were prepared by placing a droplet of sample suspension on a formvar coated TEM grid and left for 5–10 s. Subsequently, the grid was washed in ultra-deionised water and water droplets were removed with the edge of a paper towel.

Results and Discussion

Energy of binding. The force spectra (Fig. 2) show that the rupture force between hematite and the OH group is ~6 times higher than between COO^- and HPO_4^- groups (Fig. 2, Table S-1). Recalculated to ΔG_{bu} (Eq. S-4), that is an increase in ~2 kT. These binding energies suggest that the interaction is dominated by strong Van der Waals or weak electrostatic forces (Israelachvili, 2011). Considering that the {0001} hematite surface is completely hydroxylated in water (Trainor *et al.*, 2004), our results follow the trend where OH-OH bonds are twice as strong as COO^--OH bonds at circumneutral pH (Vezenov *et al.*, 1997) present in Precambrian ocean. Thus, irrespective of the transformation pathway, biopolymers rich in acidic groups desorb more easily from hematite than those rich in hydroxyl groups.

Transformation pathway. To investigate the fate of a ferrihydrite-associated OH-containing molecule during transformation to hematite, we transformed the ferrihydrite-glycerol complex, monitored the transformation pathway with XRD and determined the weight loss with TGA. The ferrihydrite-glycerol complex transformed directly to hematite without any intermediate phases detectable by XRD (Fig. S-3) suggesting a solid-state transformation pathway. As a control, we transformed ferrihydrite in absence of glycerol using the same solution conditions. Even though the hematite was the first phase to occur after 17 hr, goethite started forming after 43 hr (Fig. S-2) indicating that, in pure systems, some ferrihydrite dissolves and reprecipitates as goethite, as previously shown (Das *et al.*, 2011).

The transformation is accompanied by glycerol release. In general, the ferrihydrite-gycerol complex lost more weight than the pure ferrihydrite (Fig. 3, Table 1). Ferrihydrite is more

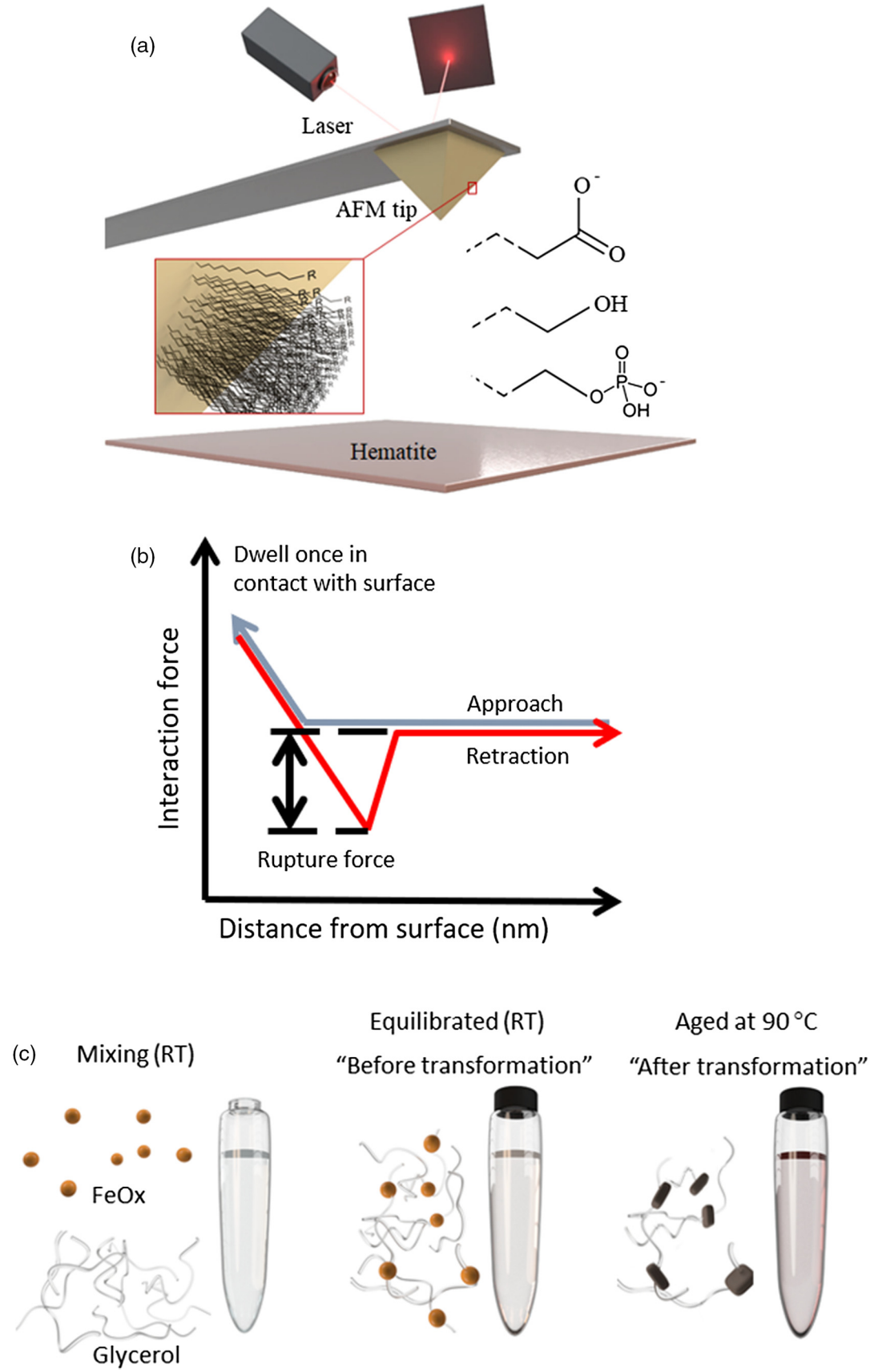

Figure 1 **(a)** Schematics of the DFS (Dynamic Force Spectroscopy): self assembled monolayers with carboxyl, hydroxyl and phosphate head-groups covalently bonded to AFM tip. **(b)** A scheme of a force curve. **(c)** In transformation experiments, ferrihydrite and glycerol were mixed at room temperature and left to equilibrate overnight. One sample was then taken for TGA (equilibrated sample) and the rest was placed in the oven at 90 °C until the transformation was complete (aged sample).

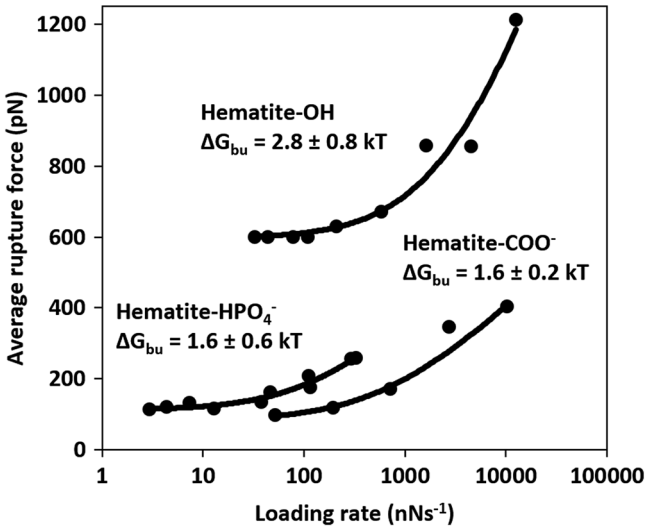

Figure 2 Multibond fit (Friddle *et al.*, 2012) to the dynamic force spectra between hematite surface and alkyl thiol self assembled monolayers with OH, HPO_4^- and COO^- head groups. The uncertainty represents the error propagated from the standard deviations of the fit. Loading rate is a nominal retraction velocity (nms^{-1}) multiplied with the spring constant of the cantilever (nNnm^{-1}).

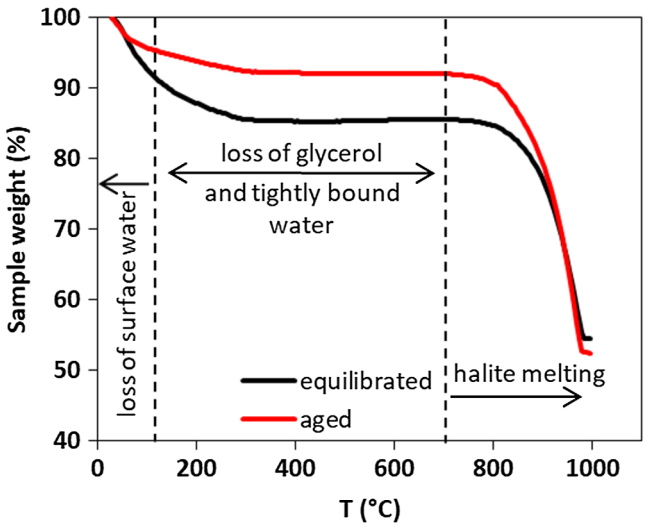

Figure 3 Comparison of thermogravimetry curves of ferrihydrite-glycerol (equilibrium-black curve) and resulting hematite-glycerol (aged-red curve). The smaller mass loss in the region 125–700 °C (dashed vertical lines) for the aged sample compared to the equilibrium sample suggests bigger loss of tightly bound water and glycerol during the transformation.

Table 1 Weight loss during the TGA analysis in <125 °C and 125–700 °C regions.

Sample		% weight loss	
		<125 °C	125–700 °C
Glycerol	equilibrated	8.9	5.4
	aged	4.8	3.2
Control	equilibrated	9.8	4.7
	aged	n.a.*	n.a.

* transformation yielded both goethite and hematite making comparison impossible

hydrated than hematite so the loss of loosely adsorbed water (<125 °C) and tightly bound water (125–700 °C) is higher for ferrihydrite than hematite (Hiemstra and Van Riemsdijk, 2009). Comparing the weight loss of ferrihydrite-glycerol (5.4 %; Table 1) to pure ferrihydrite (4.7 %) in the 125–700 °C range, shows that the tightly bound water accounts only for 87 % of the weight loss in this region, indicating that the remaining 13 % is the loss of glycerol and associated interfacial water. This implies that hematite produced by aging ferrihydrite-glycerol contains less glycerol than the original ferrihydrite-glycerol (equilibrated), and that glycerol is released during transformation. Considering that the initial amount of adsorbed glycerol is ~5 mg/g of ferrihydrite (Fig. S-1), TGA indicates that all glycerol has been desorbed during the transformation.

The reason for the loss of the glycerol during transformation can also be the smaller specific surface area (SSA) of the produced hematite (Fig. S-4) and not only the lower affinity for glycerol compared to ferrihydrite. From TEM images, we estimated the SSA of ferrihydrite to be 374–790 m^2g^{-1} and of hematite to be 10–46 m^2g^{-1}. Thus, the decrease in the SSA because of grain coarsening during transformation is between 9–70 times which alone might explain the decrease in glycerol content. However, the loss must be amplified by the lower ΔG_{bu} for hematite-OH than for ferrihydrite-OH system. In addition, our thermodynamic results suggest that the loss of organic compounds would have happened because of decreased ΔG_{bu} even if the subsequent grain coarsening does not occur, *e.g.*, in case of hematite growth inhibition caused by organic compounds. However, both scenarios are likely to have contributed to the loss of organic compounds during the formation of IFs.

We have demonstrated that glycerol, a molecule with a high ΔG_{bu} to hematite, desorbs during the transformation of ferrihydrite to hematite. We propose that a significant mass of organic compounds from FeOx-EPS composites is desorbed early in the process of FeOx sedimentation because of the transformation from ferrihydrite to hematite. This loss of organic compounds is probably further enhanced by the grain coarsening of hematite during diagenetic and metamorphic processes and concomitant reactions in the microenvironment that result in secondary mineralisation, *e.g.*, Posth *et al.* (2013). Our experiments were designed to determine the loss of strongly bound molecules from FeOx during the direct transformation, which is least likely to result in desorption of adsorbed organic compounds. The less strongly bound organic compounds or organic compounds adsorbed to ferrihydrite that transformed *via* dissolution-precipitation pathway would likely have desorbed in higher proportion than that we report here. Thus, our results highlight that the absence of organic compounds in IF should not be used as evidence against their biogenic origin.

Acknowledgements

We thank Heloisa N. Bordallo for access to TGA instrument (Carlsbergfondets, grant no. 2013_01_0589). KKS and ACM are grateful for funding from the European Union's Horizon 2020 Research and Innovation Programme under Marie Skłodowska-Curie Grant Agreement No 663830 and the Welsh Government and Higher Education Funding Council for Wales through the Sêr Cymru National Research Network for Low Carbon, Energy and Environment. KKS is grateful for funding from the Danish Council for Independent Research Sapere Aude Programs (0602-02654B).

Editor: Karim Benzerara

Additional Information

Supplementary Information accompanies this letter at http://www.geochemicalperspectivesletters.org/article2030.

Cite this letter as: Jelavić, S., Mitchell, A.C., Sand, K.K. (2020) Fate of organic compounds during transformation of ferrihydrite in iron formations. *Geochem. Persp. Let.* 15, 25–29.

References

Chan, C.S., Stasio, G.D., Welch, S.A., Girasole, M., Frazer, B.H., Nesterova, M.V., Fakra, S., Banfield, J.F. (2004) Microbial Polysaccharides Template Assembly of Nanocrystal Fibers. *Science* 303, 1656–1658.

Chen, C., Kukkadapu, R., Sparks, D.L. (2015) Influence of Coprecipitated Organic Matter on $Fe^{2+}_{(aq)}$-Catalyzed Transformation of Ferrihydrite: Implications for Carbon Dynamics. *Environmental Science & Technology* 49, 10927–10936.

Cornell, R.M., Schwertmann, U. (2004) Crystal Morphology and Size. In: *The Iron Oxides.* Wiley-VCH Verlag Gmbh & Co., Weinheim, 59–94.

Cudennec, Y., Lecerf, A. (2006) The transformation of ferrihydrite into goethite or hematite, revisited. *Journal of Solid State Chemistry* 179, 716–722.

Das, S., Hendry, M.J., Essilfie-Dughan, J. (2011) Transformation of Two-Line Ferrihydrite to Goethite and Hematite as a Function of pH and Temperature. *Environmental Science & Technology* 45, 268–275.

Dodd, M.S., Papineau, D., Pirajno, F., Wan, Y., Karhu, J.A. (2019) Minimal biomass deposition in banded iron formations inferred from organic matter and clay relationships. *Nature Communications* 10, 1–13.

Friddle, R.W., Noy, A., Yoreo, J.J.D. (2012) Interpreting the widespread nonlinear force spectra of intermolecular bonds. *Proceedings of the National Academy of Sciences* 109, 13573–13578.

Garrels, R.M., Perry, E.A., Mackenzie, F.T. (1973) Genesis of Precambrian Iron-Formations and the Development of Atmospheric Oxygen. *Economic Geology* 68, 1173–1179.

Halama, M., Swanner, E.D., Konhauser, K.O., Kappler, A. (2016) Evaluation of siderite and magnetite formation in BIFs by pressure–temperature experiments of Fe(III) minerals and microbial biomass. *Earth and Planetary Science Letters* 450, 243–253.

Hansel, C.M., Benner, S.G., Neiss, J., Dohnalkova, A., Kukkadapu, R.K., Fendorf, S. (2003) Secondary mineralization pathways induced by dissimilatory iron reduction of ferrihydrite under advective flow. *Geochimica et Cosmochimica Acta* 67, 2977–2992.

Hartman, P. (1989) The effect of surface relaxation on crystal habit: Cases of corundum (α-Al_2O_3) and Hematite (α-Fe_2O_3). *Journal of Crystal Growth* 96, 667–672.

Hegler, F., Posth, N.R., Jiang, J., Kappler, A. (2008) Physiology of phototrophic iron(II)-oxidizing bacteria: implications for modern and ancient environments. *FEMS Microbiology Ecology* 66, 250–260.

Hiemstra, T., Van Riemsdijk, W.H. (2009) A surface structural model for ferrihydrite I: Sites related to primary charge, molar mass, and mass density. *Geochimica et Cosmochimica Acta* 73, 4423–4436.

Israelachvili, J.N. (2011) *Intermolecular and Surface Forces*. Third edition, Elsevier, Burlington.

Jelavić, S., Tobler, D.J., Hassenkam, T., Yoreo, J.J.D., Stipp, S.L.S., Sand, K.K. (2017) Prebiotic RNA polymerisation: energetics of nucleotide adsorption and polymerisation on clay mineral surfaces. *Chemical Communications* 53, 12700–12703.

Kappler, A., Pasquero, C., Konhauser, K.O., Newman, D.K. (2005) Deposition of banded iron formations by anoxygenic phototrophic Fe(II)-oxidizing bacteria. *Geology* 33, 865–868.

Kleber, M., Eusterhues, K., Keiluweit, M., Mikutta, C., Mikutta, R., Nico, P.S. (2015) Chapter One – Mineral–Organic Associations: Formation, Properties, and Relevance in Soil Environments. In: Sparks, D.L. (Ed.) *Advances in Agronomy*. Academic Press, Cambridge, 1–140.

Klein, C. (2005) Some Precambrian banded iron-formations (BIFs) from around the world: Their age, geologic setting, mineralogy, metamorphism, geochemistry, and origins. *American Mineralogist* 90, 1473–1499.

Koehler, I., Konhauser, K., Kappler, A. (2010) Role of Microorganisms in Banded Iron Formations. In: Barton, L.L., Mandl, M., Loy, A (Eds.) *Geomicrobiology: Molecular and Environmental Perspective*. Springer Netherlands, Dordrecht, 309–324.

Köhler, I., Konhauser, K.O., Papineau, D., Bekker, A., Kappler, A. (2013) Biological carbon precursor to diagenetic siderite with spherical structures in iron formations. *Nature Communications* 4, 1–7.

Konhauser, K.O., Planavsky, N.J., Hardisty, D.S., Robbins, L.J., Warchola, T.J., Haugaard, R., Lalonde, S.V., Partin, C.A., Oonk, P.B.H., Tsikos, H., Lyons, T.W., Bekker, A., Johnson, C.M. (2017) Iron formations: A global record of Neoarchaean to Palaeoproterozoic environmental history. *Earth-Science Reviews* 172, 140–177.

Lützenkirchen, J., Preočanin, T., Stipić, F., Heberling, F., Rosenqvist, J., Kallay, N. (2013) Surface potential at the hematite (001) crystal plane in aqueous environments and the effects of prolonged aging in water. *Geochimica et Cosmochimica Acta* 120, 479–486.

Mikutta, R., Lorenz, D., Guggenberger, G., Haumaier, L., Freund, A. (2014) Properties and reactivity of Fe-organic matter associations formed by coprecipitation versus adsorption: Clues from arsenate batch adsorption. *Geochimica et Cosmochimica Acta* 144, 258–276.

Newcomb, C.J., Qafoku, N.P., Grate, J.W., Bailey, V.L., Yoreo, J.J.D. (2017) Developing a molecular picture of soil organic matter–mineral interactions by quantifying organo–mineral binding. *Nature Communications* 8, 396.

Phoenix, V.R., Adams, D.G., Konhauser, K.O. (2000) Cyanobacterial viability during hydrothermal biomineralisation. *Chemical Geology* 169, 329–338.

Posth, N.R., Köhler, I., Swanner, E.D., Schröder, C., Wellmann, E., Binder, B., Konhauser, K.O., Neumann, U., Berthold, C., Nowak, M., Kappler, A. (2013) Simulating Precambrian banded iron formation diagenesis. *Chemical Geology*, Special Issue dedicated to H.D. Holland: Evolution of the atmosphere and ocean through time 362, 66–73.

Sand, K.K., Jelavić, S., Dobberschütz, S., Ashby, P.D., Marshall, M.J., Dideriksen, K., Stipp, S.L.S., Kerisit, S.N., Friddle, R.W., DeYoreo, J.J. (2020) Mechanistic insight into biopolymer induced iron oxide mineralization through quantification of molecular bonding. *Nanoscale Advances* 2, 3323–3333.

Schwertmann, U., Cornell, R.M. (2000) Ferrihydrite. In: *Iron Oxides in the Laboratory*. John Wiley & Sons, Ltd, Weinheim, 103–112.

Schwertmann, U., Murad, E. (1983) Effect of pH on the Formation of Goethite and Hematite from Ferrihydrite. *Clays and Clay Minerals* 31, 277–284.

Sun, S., Konhauser, K.O., Kappler, A., Li, Y.-L. (2015) Primary hematite in Neoarchean to Paleoproterozoic oceans. *GSA Bulletin* 127, 850–861.

Trainor, T.P., Chaka, A.M., Eng, P.J., Newville, M., Waychunas, G.A., Catalano, J.G., Brown, G.E. (2004) Structure and reactivity of the hydrated hematite (0001) surface. *Surface Science* 573, 204–224.

van Oss, C.J. (1997) Hydrophobicity and hydrophilicity of biosurfaces. *Current Opinion in Colloid & Interface Science* 2, 503–512.

Vezenov, D.V., Noy, A., Rozsnyai, L.F., Lieber, C.M. (1997) Force Titrations and Ionization State Sensitive Imaging of Functional Groups in Aqueous Solutions by Chemical Force Microscopy. *Journal of the American Chemical Society* 119, 2006–2015.

Geochemical Perspectives Letters

Fate of organic compounds during transformation of ferrihydrite in iron formations

S. Jelavić, A.C. Mitchell, K.K. Sand

Supplementary Information

The Supplementary Information includes:

- Tip Functionalisation
- Cleaning of Hematite Substrate
- Dynamic Force Spectroscopy (DFS)
- The effect of temperature on ΔG_{bu}
- Estimating the adsorption capacity of ferrihydrite for glycerol
- X-ray Diffraction (XRD)
- Estimation of the Specific Surface Area (SSA)
- Supplementary Information References

Tip Functionalisation

Tips were cleaned in the UV/ozone chamber for 20 min and functionalized by placing them in 1 mM ethanol (anhydrous, ≥99.5 %, Sigma-Aldrich) solution of 11-mercaptoundecanoic acid (HS-$(CH_2)_{10}$COOH, 95 %, Sigma-Aldrich) with 10 wt.% of anhydrous acetic acid (≥99 %, Sigma Aldrich) for preparation of carboxylic tips, 11-mercaptoundecylphosphoric acid (HS-$(CH_2)_{11}H_2PO_4$, 90 %; Sigma-Aldrich) for phosphate tips or 11-mercapto-1-undecanol (HS-$(CH_2)_{11}$OH, 99 %, Sigma-Aldrich) for preparation of alcohol tips. Tips were left in a thiol solution overnight to form a self-assembled monolayer (SAM) where –COOH, –OH or $–OPO_3H_2$ headgroups point away from the AFM probe and into the solution. Excess thiols were rinsed by keeping the tips in ethanol (anhydrous, ≥99.5 %, Sigma-Aldrich) for 20 min immediately prior to their use.

Cleaning of Hematite Substrate

We washed the hematite substrate in 1 M NaOH (≥98 %, Sigma Aldrich) maintained at 60 ºC for 1 hour. Subsequently, we sonicated the solution for 20 minutes to remove the particulate contamination, washed the substrates under flowing MiliQ (ultradeionised water, resistivity >18.2 MΩcm), dried it with N_2 and placed in an UV/ozone chamber for 30 min to remove the adventitious carbon (organic compounds adsorbed from air or solution). A fully hydrated {0001} hematite surface, as encountered in aqueous solutions, predominantly consists of hydroxylated terminal Fe and O in similar proportions (~50:50) (Trainor *et al*., 2004; Tanwar *et al*., 2009*)*, where the hydroxyls are mainly doubly coordinated (Barrón and Torrent, 1996; Eggleston *et al*., 2003).

Dynamic Force Spectroscopy (DFS)

Dynamic Forces Spectroscopy (DFS) is a technique of Atomic Force Microscopy (AFM) that relies on formation of a bond between the AFM probe and the mineral surface (Fig. 1a). Here, we have decorated the probe with organic functional groups. Once the bond between the molecules at the functionalized probe and the surface is formed, the bond is forcefully broken and the rupture force measured as a function of distance between the probe and the surface. One cycle of the tip approaching, dwelling and retracting from the surface is called a force curve (Fig. 1b). A discontinuity in the retraction path of the force curve represents the rupture of a bond. The rupture force is not an intrinsic property of the bond but depends on the velocity by which the tip and the mineral surface are separated i.e. the rupture forces increase as the retraction velocity increases (Evans and Ritchie, 1997).

The retraction velocities are recalculated to loading rates, r, defined as $r=kv$, where k represents the spring constant of the AFM cantilever and v represents the retraction velocity of the tip. The plot of recorded rupture forces as a function of loading rate is called a force spectrum (*e.g*., Fig. 2) that is defined by the near-equilibrium and kinetic regimes. In the near-equilibrium regime, the loading rate is so slow that the rates of bond forming and breaking are equal. This regime is characterised by rupture forces being independent of the loading rate, *i.e.* the force spectrum curve is subparallel to the *y*-axis. In the kinetic regime, the rate of bond breaking is faster than the rate of bond forming. This regime is characterised by rupture forces increasing exponentially with the increase in loading rate.

We then fit these two regimes to a multibond model (Friddle *et al*., 2012) defined as:

$$\langle f \rangle \cong f_{eq} + f_{\beta}^{app} \ln\left(1 + e^{-\gamma} R(f_{eq})\right), \quad \text{Eq. S-1}$$

$$f_{\beta}^{app} = N \frac{k_B T}{x_t}, \quad \text{Eq. S-2}$$

$$R(f_{eq}/N) = \frac{r}{f_{\beta}^{app} k_{off} f_{eq}}, \quad \text{Eq. S-3}$$

where f represents the rupture force, f_{eq} the equilibrium rupture force, γ the Euler constant, N the number of interacting bonds, k_B the Boltzmann constant, T the temperature, x_t the distance between the energy minimum of a bound and the transition state and k_{off} represents the intrinsic kinetic unbinding (off) rate. f_{eq}, x_t and k_{off}

are binding parameters that define the energy landscape of a bond. The bond parameters determined in this study are given in Table S-1.

Table S-1 Bond parameters.

	Hematite – HPO_4^-	Hematite – COO^-	Hematite – OH
x_t (Å)	0.4 ± 0.3	0.40 ± 0.04	0.10 ± 0.04
k_{off} (s^{-1})	241 ± 352	1934 ± 570	1351 ± 1360
f_{eq} (pN)	104 ± 18	83 ± 8	597 ± 18

* uncertainty expressed as a standard deviation

Usually, not one but many bonds form between the tip and the surface, thus the recorded rupture forces represent breaking of an undefined ensemble of bonds, which complicates comparison among tips functionalised with different functional groups. However, this problem can be circumvented by comparing the Gibbs free energy of binding (ΔG_{bu}) derived from bond parameters. f_{eq} and x_t are used to calculate ΔG_{bu} through (Friddle *et al.*, 2012):

$$\Delta G_{bu} = k_B T \ln \frac{f_{eq} x_t}{k_B T} + f_{eq} x_t + k_B T. \qquad \text{Eq. S-4}$$

The bond strength between organic compounds and mineral surfaces depends on the composition of the surrounding solution, in particular the pH and the ionic strength. We have conducted our DFS experiments at pH=5.5 and at 10 mM NaCl. Our pH is for ~1.5 unit lower than the current estimates for Precambrian seawater (Halevy and Bachan, 2017; Krissansen-Totton *et al.*, 2018). However, we chose this pH because the surface potential of hematite {0001} is mostly neutral and the zeta potential is slightly positive (Lützenkirchen *et al.*, 2013), which resembles the surface properties of particulate hematite at circumneutral conditions (Kosmulski, 2009) present during the Precambrian. We used a solution concentration of 10 mM instead of higher concentration typical for seawater to maximize the interactions (Newcomb *et al.*, 2017). We chose not to work with solution similar to seawater because we wanted to avoid issues with high activities of divalent cations.

For all DFS measurements, the spring constant of the probe was calculated using a thermal calibration method (Hutter and Bechhoefer, 1993). Our ΔG_{bu} are comparable to values between goethite and COO^- (1.0 ± 0.6 kT), and goethite and PO_3^- (1.6 ± 0.9 kT) obtained at similar solution conditions (Newcomb *et al.*, 2017).

The Effect of Temperature on ΔG_{bu}

From van't Hoff's equation (Denbigh, 1981), it follows that for exothermic reactions, ΔG_{bu} decreases with increasing temperature. This implies that at the temperatures such were common in Precambrian oceans, i.e. 50-85 °C (Knauth, 2005; Robert and Chaussidon, 2006; Garcia *et al.*, 2017), the binding between organic functional groups and iron (oxyhydr)oxides was weaker compared to binding at the temperature at which the DFS experiments were conducted. In addition, an increase in temperature results in a decrease in the point of zero charge of iron (oxyhydr)oxides (Rodda *et al.*, 1993) again suggesting weaker binding to carboxyl, phosphate and hydroxyl functional groups (Newcomb *et al.*, 2017) if the interactions are purely electrostatic (Sposito, 2004). Combined, the binding between organic functional groups and iron (oxyhydr)oxides was weaker in Precambrian oceans than at room temperature experiments implying even higher desorption of

organic compounds during mineral transformation than shown in our experiments. This reinforces our hypothesis that the organic compounds were largely absent from iron formations since their deposition.

Estimating the Adsorption Capacity of Ferrihydrite for Glycerol

To estimate the adsorption capacity of ferrihydrite for glycerol, we conducted batch experiments. The samples were prepared in the same way as the samples for transformation experiments except they were not washed. After centrifugation, the supernatant was collected and the concentration of glycerol measured with spectrophotometry (Bondioli and Bella, 2005). In short, the glycerol was oxidised with sodium periodate ($NaIO_4$, Sigma Aldrich, ≥99.8 %) to formaldehyde (CH_2O), which was subsequently reacted with acetylacetone ($(CH_3)_2(CO)_2CH_2$, Merck, ≥99 %) in presence of ammonium acetate ($NH_4CH_3CO_2$) as a source of N to give highly absorptive complex (410 nm) 3,5-diacetyl-1,4-dihydrolutidine ($C_{11}H_{15}NO_2$). The absorption of the complex was measured using Thermo Scientific Multiskan Microplate Spectrophotometer. We prepared 7 standards (0.064, 0.036, 0.024, 0.018, 0.0135, 0.009 and 0.0045 $mgml^{-1}$) and a blank sample to calibrate the instrument. The samples were prepared in triplicates and the analysis of samples, standards and the blank were repeated twice to account for the instrumental uncertainty.

Figure S-1 shows the adsorption isotherm and the corresponding Freundlich fit to the data. Based on these results, we decided to conduct transformation experiments at glycerol concentration of 0.5 % which corresponds to the equilibrium concentration of ~ Ce= 1000 mgL^{-1}. We chose to do so to minimise the intermolecular interactions that do not influence the glycerol-ferrihydrite binding energy but would significantly decrease the transformation rates.

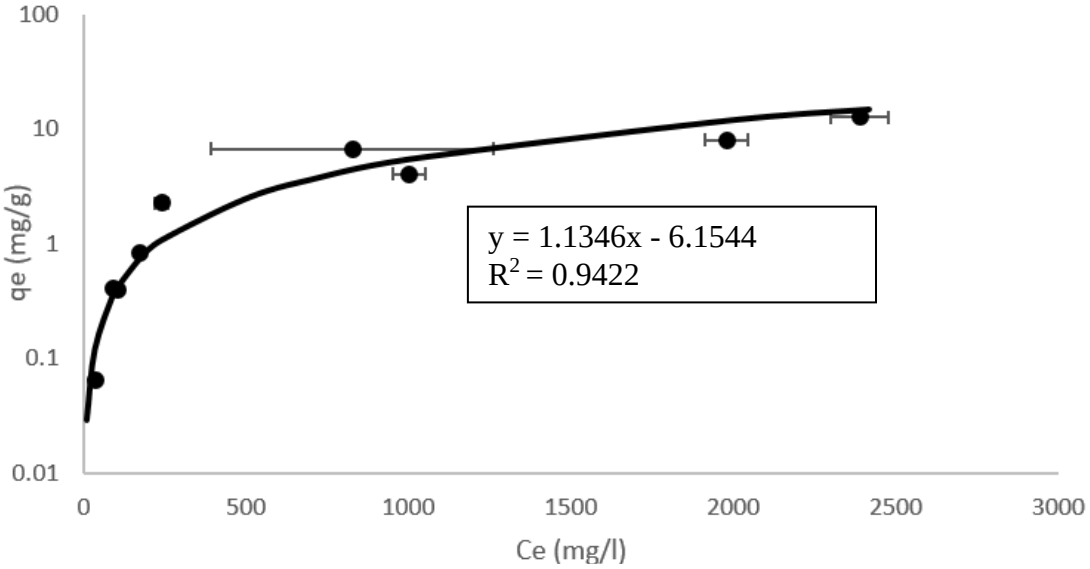

Figure S-1 Adsorption isotherm of glycerol on ferrihydrite and the corresponding Freundlich fit. q_e represents the mass of adsorbed glycerol per gram of ferrihydrite and C_e represents the equilibrium concentration of glycerol in contact with ferrihdyrite. Insert represents the equation of the fit and the R^2 represents the coefficient of determination. Uncertainties are shown as standard deviations. The uncertainty for q_e are smaller than the size of a symbol.

X-ray Diffraction (XRD)

To maximise diffracted intensities from a small amount of material, the instrumental profile was set in such a way which resulted in the diameter of the incident X-rays being longer than the diameter of the zero background Si plate. This meant that there was some diffused scattering arising from the surrounding poly(methyl methacrylate) holder. To remove that diffused contribution, we have subtracted a diffractogram of a blank poly(methyl methacrylate) holder from each measured sample.

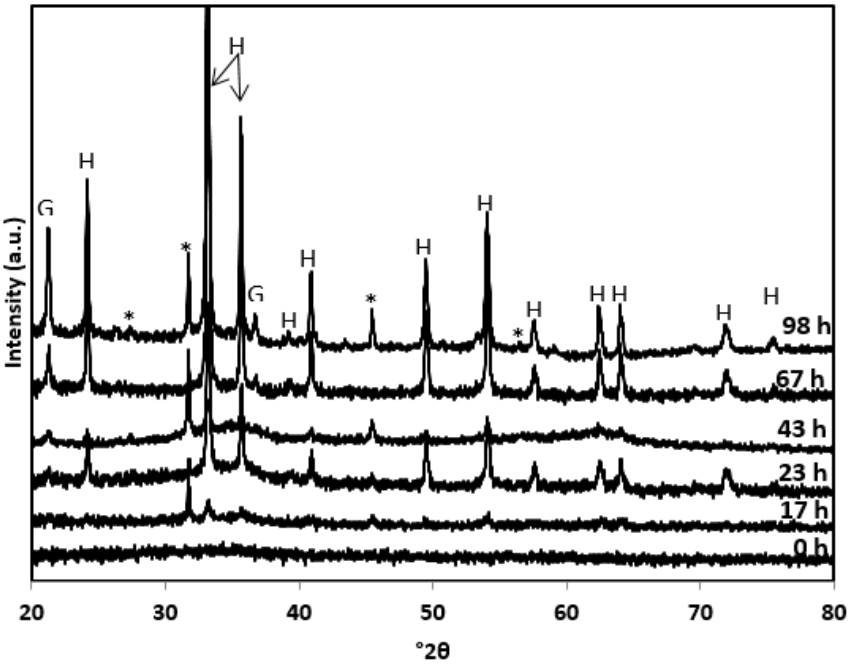

Figure S-2 X-ray diffractograms for the succesive samples (0-98 h) obtained by aging ferrihydrite in 0.5 M NaCl solution at 90 °C. The diffractogram at 0 h was collected on a sample that was equilibrated overnight and analysed immediately. The diffractogram of the product obtained after 98 h of aging shows reflections of goethite (G), hematite (H) and halite (*). Halite is present in samples in which it was not possible to completely remove it by washing with MiliQ. Diffractograms are scaled along the *y*-axis for clarity.

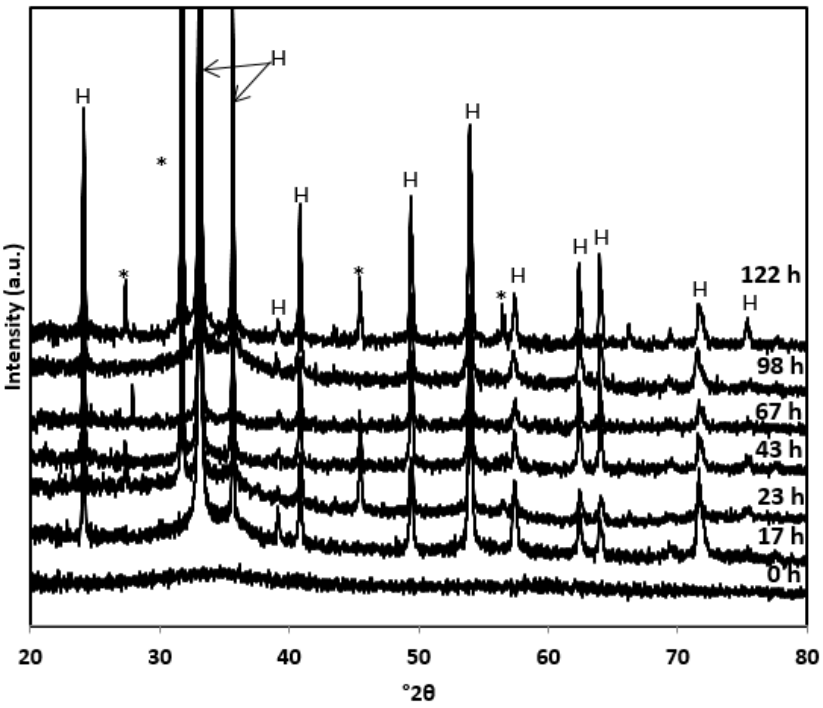

Figure S-3 X-ray diffractograms for the succesive samples (0-120 h) obtained by aging ferrihydrite in 0.5 M NaCl solution at 90 °C in presence of glycerol. The diffractogram at 0 h was collected on a sample that was equilibrated overnight and analysed immediately. The only FeOx species present in the product after 120 h of aging is hematite (H). Halite is present in samples in which it was not possible to completely remove it by washing. Diffractograms are scaled along the *y*-axis for clarity.

Estimation of the Specific Surface Area (SSA)

We estimated the SSA of the precursor ferrihydrite and produced hematite by assuming an ideal, non porous spherical shape of ferrihydrite particles and by taking an average of observed particle dimensions of hematite. Our TEM images are not of sufficient resolution to directly measure the diameter of ferrihydrite particles but we know that our precursor ferrihydrite is "2-line" (Figs. S-2 and S-3). The maximum observed size for 2-line ferrihydrite is 3 nm (Janney *et al.*, 2000) so we calculated the range of possible SSA's by taking:

$$\boldsymbol{SSA\ (ferrihydrite)} = \frac{\boldsymbol{6}}{\boldsymbol{\rho d}}, \qquad \text{Eq. S-5}$$

where ρ represents the mass density of ferrihydrite taken as 3.8 gcm^{-3} and d represents the particle diameter (between 2-3 nm). This gave values of SSA for ferrihydrite between 526-790 m^{2}g^{-1}.

The SSA for hematite was estimated by taking:

$$\boldsymbol{SSA\ (hematite)} = \frac{\boldsymbol{2lw + 2lt + 2tw}}{\boldsymbol{\rho abc}}, \qquad \text{Eq. S-6}$$

where *l* represents the average of observed particle lengths, *w* represents the average of particle widths and *t* represents the assumed particle thickness. We took a minimum particle thickness to be 10 nm and maximum to be equal to the average of observed particle widths. This gave estimated SSA for hematite product in range of 11-46 m^2g^{-1}.

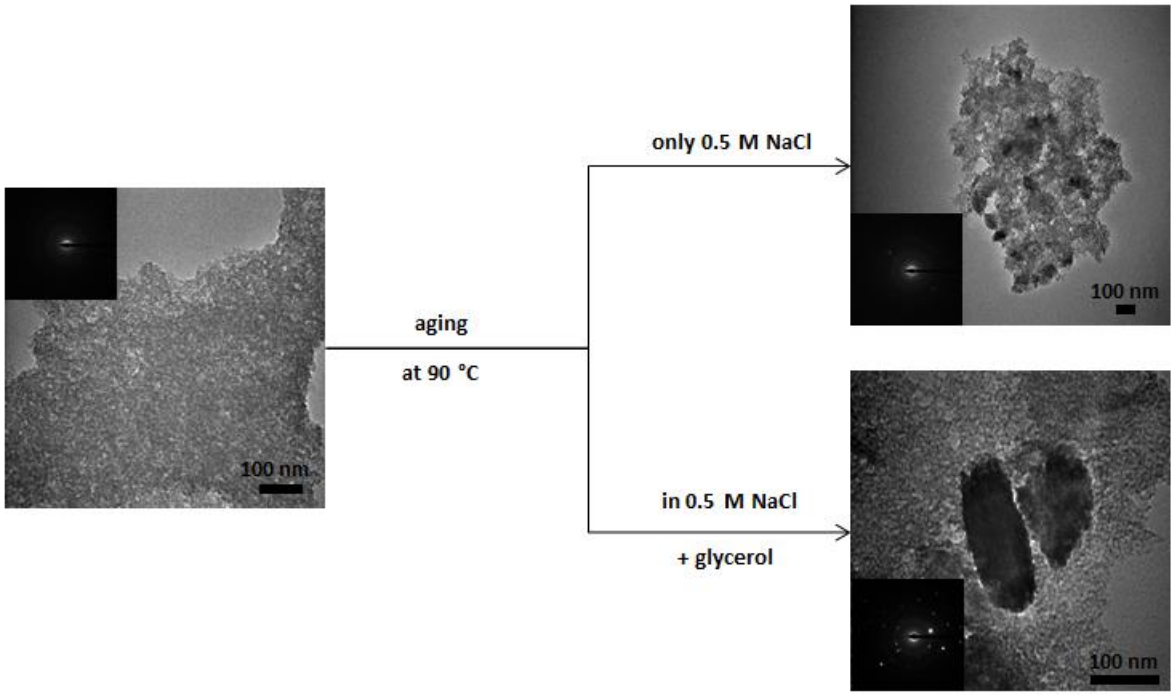

Figure S-4 TEM images of ferrihydrite precursor (left), ferrihydrite aged in 0.5 M NaCl solution (upper right) and ferrihydrite aged in 0.5 M NaCl and 0.5 % glycerol.

Supplementary Information References

Barrón, V., Torrent, J. (1996) Surface Hydroxyl Configuration of Various Crystal Faces of Hematite and Goethite. *Journal of Colloid and Interface Science* 177, 407–410.

Bondioli, P., Bella, L.D. (2005) An alternative spectrophotometric method for the determination of free glycerol in biodiesel. *European Journal of Lipid Science and Technology* 107, 153–157.

Denbigh, K.G. (1981) Equilibria of Reactions Involving Gases. In: *The Principles of Chemical Equilibrium: With Applications in Chemistry and Chemical Engineering*. Cambridge University Press, Cambridge, 133–181.

Eggleston, C.M., Stack, A.G., Rosso, K.M., Higgins, S.R., Bice, A.M., Boese, S.W., Pribyl, R.D., Nichols, J.J. (2003) The structure of hematite (α-Fe_2O_3) (001) surfaces in aqueous media: scanning tunneling microscopy and resonant tunneling calculations of coexisting O and Fe terminations. *Geochimica et Cosmochimica Acta* 67, 985–1000.

Evans, E., Ritchie, K. (1997) Dynamic strength of molecular adhesion bonds. *Biophysical Journal* 72, 1541–1555.

Friddle, R.W., Noy, A., Yoreo, J.J.D. (2012) Interpreting the widespread nonlinear force spectra of intermolecular bonds. *Proceedings of the National Academy of Sciences* 109, 13573–13578.

Garcia, A.K., Schopf, J.W., Yokobori, S., Akanuma, S., Yamagishi, A. (2017) Reconstructed ancestral enzymes suggest long-term cooling of Earth's photic zone since the Archean. *Proceedings of the National Academy of Sciences* 114, 4619–4624.

Halevy, I., Bachan, A. (2017) The geologic history of seawater pH. *Science* 355, 1069–1071.

Hutter, J.L., Bechhoefer, J. (1993) Calibration of atomic-force microscope tips. *Review of Scientific Instruments* 64, 1868–1873.

Janney, D.E., Cowley, J.M., Buseck, P.R. (2000) Transmission Electron Microscopy of Synthetic 2- and 6-Line Ferrihydrite. *Clays and Clay Minerals* 48, 111–119.

Knauth, L.P. (2005) Temperature and salinity history of the Precambrian ocean: implications for the course of microbial evolution. *Palaeogeography, Palaeoclimatology, Palaeoecology*, Geobiology: Objectives, Concept, Perspectives 219, 53–69.

Kosmulski, M. (2009) *Surface Charging and Points of Zero Charge*. CRC Press, Boca Raton.

Krissansen-Totton, J., Arney, G.N., Catling, D.C. (2018) Constraining the climate and ocean pH of the early Earth with a geological carbon cycle model. *Proceedings of the National Academy of Sciences* 115, 4105–4110.

Lützenkirchen, J., Preočanin, T., Stipić, F., Heberling, F., Rosenqvist, J., Kallay, N. (2013) Surface potential at the hematite (001) crystal plane in aqueous environments and the effects of prolonged aging in water. *Geochimica et Cosmochimica Acta* 120, 479–486.

Newcomb, C.J., Qafoku, N.P., Grate, J.W., Bailey, V.L., Yoreo, J.J.D. (2017) Developing a molecular picture of soil organic matter–mineral interactions by quantifying organo–mineral binding. *Nature Communications* 8, 396.

Robert, F., Chaussidon, M. (2006) A palaeotemperature curve for the Precambrian oceans based on silicon isotopes in cherts. *Nature* 443, 969–972.

Rodda, D.P., Johnson, B.B., Wells, J.D. (1993) The Effect of Temperature and pH on the Adsorption of Copper (II), Lead (II), and Zinc (II) onto Goethite. *Journal of Colloid and Interface Science* 161, 57–62.

Sposito, G. (2004) *The Surface Chemistry of Natural Particles*. Oxford University Press, New York.

Tanwar, K.S., Petitto, S.C., Ghose, S.K., Eng, P.J., Trainor, T.P. (2009) Fe (II) adsorption on hematite (0001). *Geochimica et Cosmochimica Acta* 73, 4346–4365.

Trainor, T.P., Chaka, A.M., Eng, P.J., Newville, M., Waychunas, G.A., Catalano, J.G., Brown, G.E. (2004) Structure and reactivity of the hydrated hematite (0001) surface. *Surface Science* 573, 204–224.